Chemical Engineering Journal 499 (2024) 155852

Contents lists available at ScienceDirect

Chemical Engineering Journal

journal homepage: www.elsevier.com/locate/cej

Temperature-dependent frequency control of TWC operation for efficient CH_4 and NO_x abatement of stoichiometric natural gas engines

Daniel Hodonj [a], Barbara Thiele [a], Olaf Deutschmann [a,b], Patrick Lott [a,*]

[a] Institute for Chemical Technology and Polymer Chemistry (ITCP), Karlsruhe Institute of Technology (KIT), Engesserstr. 20, 76131 Karlsruhe, Germany
[b] Institute of Catalysis Research and Technology (IKFT), Karlsruhe Institute of Technology (KIT), Hermann-von-Helmholtz-Platz 1, 76344 Eggenstein-Leopoldshafen, Germany

ARTICLE INFO

Keywords:
Dithering
Natural gas engine
Periodic operation
Three-way catalyst

ABSTRACT

A novel approach to optimize the cold start performance of Pd- and Pt-based three-way catalysts in stoichiometric natural gas engine tailpipes is presented, utilizing temperature-dependent frequency control of lambda switches. In comparison to Pt/Al_2O_3, Pd/Al_2O_3 exhibits a lower optimal frequency at the same inlet temperature, which can be attributed to the differing noble metal-specific adsorption–desorption energies of CO and O, which can inhibit the catalytic activity by surface poisoning, lower exothermicity evolving due to its lower catalytic activity and its higher oxygen storage capacity. Catalyst operation at a fixed frequency during light-off resulted in improved pollutant conversion only within a specific temperature range and relevant NH_3 slip was observed at elevated temperatures compared to conventional stoichiometric steady-state operation. In contrast, controlling the frequency as a function of the catalyst inlet temperature enabled a substantial decrease of the light-off temperature of CH_4 and NO_x and an increase in N_2 selectivity.

1. Introduction

Among other factors, transformation of the mobility sector towards near-zero emissions is a crucial prerequisite for the success of the worldwide energy transition. In addition to conceptual reorganization and expanding electromobility, it is particularly important to adapt existing technologies to environmentally friendly standards in the transportation sector [1]. Since most drive systems still rely on the combustion of gasoline-based fuels, the first step is to switch to alternative and regenerative fuels e.g. e-fuels produced from renewable energy. Methane (CH_4) is emerging as promising alternative among a wide range of options. Methane has a higher hydrogen-to-carbon ratio (H:C = 4:1) compared to conventional fuels based on long-chain hydrocarbons. This enables a reduction in CO_2 emissions during combustion. Currently, natural gas and biogas are the primary sources of CH_4. However, it is expected that the proportion of synthetic natural gas produced from renewable sources using power-to-gas strategies will increase in the future, leading to greater availability of carbon neutral methane.

Methane can be burned with excess oxygen or at a stoichiometric air–fuel equivalence ratio (AFR) of $\lambda = 1$ [2–4]. Lean-burn engines are generally more fuel efficient, but typically require a more sophisticated and expensive exhaust aftertreatment system comprising an oxidation catalyst and a catalyst for selective catalytic reduction (SCR) to efficiently reduce NO_x emissions. If stoichiometric combustion is chosen instead, a three-way catalyst (TWC) can be used to facilitate the simultaneous conversion of unburned hydrocarbons (HC), CO and NO_x, which allows for a simpler and less expensive exhaust gas aftertreatment system [5–7]. Due to its tetrahedral molecular structure, the efficient conversion of the methane molecule is a particular challenge for TWC in natural gas engines [2]. However, maximizing conversion of unburned CH_4 in the exhaust gas is crucial, as CH_4 has a greenhouse gas potential over 20 times greater than CO_2 [8].

The simultaneous catalytic conversion of NO_x presents additional challenges due to the formation of secondary emissions, namely NO_2, N_2O, and NH_3, during the reaction in the catalytic converter [9,10]. N_2O is a greenhouse gas that is estimated to have a 300 times higher greenhouse effect than CO_2 [11]. Moreover, NO_2 and NH_3 are toxic gases that can cause respiratory diseases and harm the environment [12,13]. In typical exhaust gas compositions, the efficiency of a TWC for converting pollutants is insufficient at low exhaust gas temperatures. These low temperatures occur, for example, when starting the engine or in stop-and-go situations [14,15]. Therefore, the Euro 7 emissions standard, expected to come into force in 2025, will regulate cold start behavior for the first time. Additionally, the legislator

* Corresponding author.
E-mail address: patrick.lott@kit.edu (P. Lott).

https://doi.org/10.1016/j.cej.2024.155852
Received 11 June 2024; Received in revised form 15 August 2024; Accepted 15 September 2024
Available online 17 September 2024

Nomenclature

Greek symbols		$n\tau$	Multiple of the cycle period (s)
λ	Air–fuel equivalence ratio (–)	$OSCC$	Oxygen storage capacity (μmol g^{-1})
ν_i	Stoichiometric coefficient (–)	p	Pressure (Pa)
τ	Cycle period (s)	R	Gas constant (8.314 J mol^{-1} K^{-1})
Latin symbols		S_{i,NO_x}	Selectivity derived from NO_x (–)
a_m	Area occupied by a surface atom (Å^2)	t	Time (s)
A	Amplitude (–)	T	Temperature (°C/K)
D_{PGM}	Dispersion of PGM (%)	TOF_i	Turnover frequency (s^{-1})
f	Frequency (Hz)	v_m	Volume occupied by an atom (Å^3)
$f_{opt}(T)$	Optimal frequency (Hz)	$\dot{V}$	Flow rate (m^3 s^{-1})
$GHSV$	Gas hourly space velocity (h^{-1})	X_i	Cycle-averaged conversion (–)
m_{cat}	Mass of catalyst (g)	x_{PGM}	Mass fraction of PGM (–)
M_{PGM}	Molar mass of PGM (g mol^{-1})	x_i	Species concentration (–/%/ppm)
m_{PGM}	Mass of PGM (g)	$\bar{x}_i$	Cycle-averaged mole fraction (–)

demands greater long-term stability of the exhaust gas aftertreatment system [16].

To comply with the increasingly stringent emission standards, it is necessary to improve the activity and selectivity of existing TWCs. Beyond optimization of the catalyst formulation, this improvement can be realized by introduction of efficient operation strategies. It is known that periodic changes between a lean and a rich exhaust gas composition, known as lambda-dithering, can improve the performance of Pd- and Pt-based three-way catalytic converters compared to stoichiometric steady-state operation, especially at low temperatures [17–24]. Such periodic operation is also known as lean-rich-cycling and, particularly if these lean-rich-switches occur very fast, also called lambda-dithering [25–28]. The effect of a narrow band of dithering frequency, which is characterized by the optimal frequency, which increases the conversion for each reactant above the value reached at stoichiometric steady-state operation, has not only been observed in the exhaust gas aftertreatment of gasoline engines [18,29–31], but has also been established in initial studies for natural gas engines [25,26,32–40].

TWCs are typically operated at temperatures reaching 1100 °C [41], at gas hourly space velocities (GHSVs) of 30 000–100 000 h^{-1} [42] and within an AFR range of 0.98–1.02 [5]. In addition, oxygen storage materials (OSMs) are employed to mitigate the occurrence of pollutant slip during deviations from the stoichiometric AFR. Due to the closed-loop control of fuel injection with the AFR sensor, dithering naturally occurs at a frequency of 0.5–2 Hz and at minimal amplitudes in gasoline engines [17]. Shi et al. [26] varied the amplitude in a range of 0.01–0.03 on a natural gas engine, with an amplitude of 0.03 indicating AFR oscillations between 0.97 and 1.03. However, the amplitude is constrained only by the provision of an ignitable homogeneous mixture within the cylinder [5]. For instance, amplitudes between 0.02–0.06 around the stoichiometric AFR have been investigated for forced periodic operation on gasoline engines [43,44]. Previous research has demonstrated that the frequency band which can be characterized by the optimal frequency depends on those operational conditions [18,31,45,46], variables of periodic operation [18,31,46] and oxygen storage capacity (OSC) of the catalysts [46,47].

For instance, the impact of temperature on the optimal frequency was elucidated by the observation of a temperature-dependent induction period for CO desorption when O_2 was introduced to pre-adsorbed CO on Pd/Al_2O_3 following a rich-lean switch [48]. This time delay represents the minimum cycle period necessary to achieve rate enhancement under periodic conditions [49]. Since the optimal frequency for maximum pollutant conversion increases with increasing catalyst temperature, a precise control of the optimal frequency during engine start-up could significantly reduce cold start emissions [50]. In our present study, we designed and tested a temperature-dependent dithering control system for a Pt- and Pd-based model catalyst using a realistic synthetic exhaust gas representative for a typical stoichiometric natural gas engine. The objective was to utilize the temperature-dependence of the optimal frequency for reducing cold start emissions, aiming to optimize the operation of three-way catalysts without affecting existing engine settings or conditions.

2. Methodology

2.1. Catalyst preparation

To prepare the 2 wt.-% Pd/Al_2O_3 and 2 wt.-% Pt/Al_2O_3 catalyst, γ-Al_2O_3 (Puralox TH 100/150, Sasol) was calcined in static air at 700 °C for 5 h. Subsequently, Pd and Pt were added to the calcined supports through an incipient wetness impregnation (IWI) method. For Pd/Al_2O_3, an aqueous solution of $(NH_3)_4Pd(NO_3)_2$ (abcr) was used, whereas for Pt/Al_2O_3, solid $(NH_3)_4Pt(NO_3)_2$ (Alfa Aesar) was suspended in deionized water, before drop wise addition of the precursor solution to the support while rigorously mixing. In addition, a bimetallic Pd-Pt/Al_2O_3 was prepared with a Pd and Pt loading of 1 wt.-%, respectively. For this, solid $(NH_3)_4Pt(NO_3)_2$ was suspended in the aqueous $(NH_3)_4Pd(NO_3)_2$ solution and applied analogously to the Al_2O_3 support. The impregnated powder was dried for 4 h at 70 °C and calcined in air for 5 h at 500 °C. To evaluate the catalytic activity under realistic conditions, cordierite monoliths (3 cm length, 1.6 cm diameter, 400 cpsi, 4 mil, 97 cells; Corning) were coated with the catalyst powder. Following the procedure applied by Karinshak et al. [51], the catalyst powder was mixed with AlO(OH) (Disperal P2, Sasol) in a mass ratio of 90:10 and suspended in deionized water. After acidification with aqueous HNO_3 (Fischer) the liquid slurry was added into the channels of a cordierite honeycomb by means of dip-coating and excess liquid was blown out before drying. The monolith underwent the coating procedure until reaching the desired catalyst loading of 100 g_{cat} L^{-1} (approx. 57 g_{PGM} ft^{-3}). Subsequently, the monolithic catalyst was calcined at 550 °C for 5 h in static air. To ensure a stabilized and comparably initial state of performance prior to the catalytic activity tests, the samples were de-greened at the catalyst test bench at hydrothermal conditions (10% CO_2, 10% H_2O in N_2) for 4 h at 600 °C and a $GHSV$ of 50 000 h^{-1}, following the procedure for TWC testing proposed by Rappé et al. [52].

2.2. Catalyst characterization

N_2-physisorption measurements were conducted on the catalyst powders (granulate with 125–250 μm particle size) using at a BELSORP-mini II (BEL Japan) after degassing the samples for 2 h at 300 °C. The obtained adsorption–desorption curves were evaluated using the method of Brunauer, Emmett, and Teller (BET) [53], which provides information on the specific surface area. The PGM loading of the

powder catalysts were validated using inductively coupled plasma optical emission spectroscopy (ICP-OES). To obtain the precious metal dispersion of the monolithic samples, CO chemisorption measurements were conducted in a custom-made apparatus equipped with an IR detector (X-Stream, Emerson), following procedures previously applied in the group [54]. Following oxidation in a quartz glass tubular reactor (Qsil) at 500 °C with atmospheric oxygen (O_2) for 20 min, the sample underwent reduction at 400 °C for 60 min using 5% hydrogen (H_2) in nitrogen (N_2). After cooling the reactor to room temperature under N_2 flushing, the catalyst was saturated with 1% CO in N_2 at 25 °C. Gaseous and physisorbed CO are then removed by a nitrogen stream (1 h). The CO is then desorbed by heating the sample at a rate of 20 K min^{-1} to 550 °C under inert nitrogen flow. To evaluate the precious metal dispersion, a CO:PGM adsorption ratio of 1:1 is assumed [55]. The measurement of the oxygen storage capacity complete (OSCC) is based on the aftertreatment protocols for catalyst characterization by Rappé et al. [52]. The monolithic catalyst undergoes oxidation at 550 °C with 2% O_2 in N_2 for 20 min in the test setup described below. Subsequently, the sample is cooled down to 550 °C, 350 °C, and 150 °C in N_2 and reduction is performed by switching to 1% CO in N_2. The OSCC at the given temperature represents the quantity of CO_2 produced during reduction, specified per unit mass of catalyst (cf. Eq. (1)). The theoretical value for a complete transition from PGM^{+II} to PGM^0 was calculated by the molar mass and loading of the PGMs (cf. Eq. (2)). The surface oxygen was calculated using the noble metal dispersion and the assumption of an O:Pd adsorption rate of 1:1 (cf. Eq. (3)).

$$OSCC = \frac{p\dot{V}}{RT} \cdot \frac{1}{m_{\mathrm{cat}}} \int_{t_{\mathrm{red},0}}^{t_{\mathrm{red,end}}} x_{\mathrm{CO_2}}(t)dt \tag{1}$$

$$OSCC_{\max} = \frac{x_{\mathrm{PGM}}}{M_{\mathrm{PGM}}} \tag{2}$$

$$OSCC_{\mathrm{surf}} = D_{\mathrm{PGM}} OSCC_{\max} \tag{3}$$

X-ray diffraction (XRD) patterns were recorded using a Bruker Advance D8 diffractometer, employing Cu-Kα1-radiation with a wavelength of 1.5406 Å between 2θ = 20–90° with a increment of 0.017°. The tube current was 40 mA and tube voltage 40 kV. Temperature programmed desorption of the powder samples (granulate with 125–250 µm particle size) with O_2 (O_2-TPD) and CO (CO-TPD) were performed in an AutoChem II device (micromeritics). After an oxidative pretreatment (10% O_2 in He, ramp rate of 10 K min^{-1} from room temperature to 500 °C, oxidation for 1 h) and subsequent reduction with H_2 (10% H_2 in Ar, ramp rate of 10 K min^{-1} from room temperature to 400 °C, reduction for 1 h) the samples were saturated for 1 h at 45 °C with 10% O_2 in He or 1% CO in He, respectively. To avoid H_2 adsorption on the samples, cooling down after the reduction phase was performed in He. A thermal conductivity detector (TCD) and a mass spectrometer (MS, Omnistar GSD320, Pfeiffer Vacuum) were employed to monitor the composition of the effluent gas stream while the system was flushed with 50 mL min^{-1} of pure He and heated to 600 °C with a ramp rate of 10 K min^{-1}.

2.3. Testing apparatus and procedure

The monolithic catalysts were investigated under steady-state and forced periodic conditions in an in-house built catalyst testing bench that was already, described in detail in one of our previous studies [46]. The inlet temperature of the catalyst was precisely adjusted by regulating the furnace with a Eurotherm controller, enabling samples to be subjected to temperature ramps of 5 K min^{-1} during the light-off experiments. The simulated realistic exhaust gas of a methane-fueled engine as a function of the air–fuel equivalency ratio is shown in Fig. 1. The AFR was calculated using Eq. (4) from Padeste and Baiker [31]; for the present work, the original formula was extended by a term for the methane concentration in order to account for the natural gas engine exhaust composition.

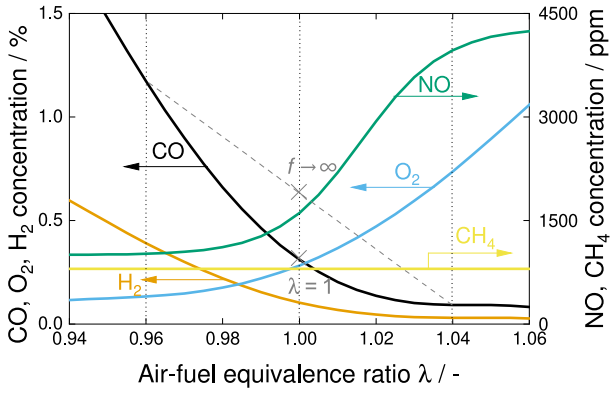

Fig. 1. Simulated O_2, CO, H_2 and NO concentrations of a methane combustion engine as a function of AFR. Components with constant concentrations: 800 ppm CH_4, 9% CO_2, 17% H_2O.

The simulated exhaust gas of the methane-fueled engine is based on the simulated exhaust gas of a gasoline engine, which was used in our previous study [46]. To reflect the higher H:C ratio of methane, the CO_2 concentration was reduced to 9% [56] and the H_2O concentration was increased to 17% [2] compared to the exhaust gas representative for typical gasoline engines [52] and in agreement with literature reports. In addition, the concentrations of CO, O_2, and HC were reduced throughout the lambda window to consider the cleaner combustion of methane compared to gasoline. The solid lines in Fig. 1 correspond to species emissions at constant AFR during steady-state operation. During periodic operation, mixing of the lean and rich phases occurs with increasing frequency due to axial dispersion, as shown by the dotted line for the CO concentration. Thus, a distinction can be made between the conventional stoichiometric steady-state, which can be accessed by operating the engine in a narrow window around $\lambda = 1$, and the fully-mixed stoichiometric steady-state, which is achieved by periodic operations at high frequencies ($f = \infty$). The catalysts were tested under the stoichiometric steady-state conditions described above, and forced periodic conditions at various frequencies and temperatures at $GHSV$ = 75 000 h^{-1} and an amplitude of $A = 0.04$, which are realistic experimental conditions that are representative for real-world TWC application [5,26,41–44].

$$\lambda = \frac{2[\mathrm{O_2}] + [\mathrm{CO}] + 2[\mathrm{CO_2}] + [\mathrm{H_2O}] + [\mathrm{NO}]}{2[\mathrm{CO}] + [\mathrm{H_2}] + 2[\mathrm{CO_2}] + [\mathrm{H_2O}] + 4[\mathrm{CH_4}]} \tag{4}$$

Cycle-average CO, NO_x, CH_4, NH_3, and N_2O concentrations were calculated by integration of the transient concentration profiles (cf. Eq. (5)) which were measured with an Fourier-transform infrared (FTIR) spectrometer (MultiGas 2030, MKS Instruments) operating at 5 Hz and with a measuring cell volume of 200 ml. Pollutant conversion and product selectivities were calculated using the cycle-average concentrations in Eqs. (6)–(7). The N_2 selectivity was calculated by a balance of all nitrogen-containing species (cf. Eq. (8)). Additionally, the inlet and outlet of the reactor have been monitored by AFR sensors (LSU 4.9, Bosch) with a sampling rate of 10 Hz.

$$\bar{x}_i = \frac{1}{n\tau} \int_{t}^{(t+n\tau)} x_i(t')dt' \tag{5}$$

$$X_i = \frac{\bar{x}_{i,0} - \bar{x}_i}{\bar{x}_{i,0}} \tag{6}$$

$$S_{i,\mathrm{NO_x}} = \frac{\nu_{\mathrm{NO_x}}}{\nu_i} \frac{\bar{x}_i - \bar{x}_{i,0}}{\bar{x}_{\mathrm{NO_x},0} - \bar{x}_{\mathrm{NO_x}}} \tag{7}$$

$$S_{\mathrm{N_2,NO_x}} = 1 - S_{\mathrm{N_2O,NO_x}} - S_{\mathrm{NH_3,NO_x}} \tag{8}$$

In order to compare the activity of Pd/Al_2O_3 and Pt/Al_2O_3 by means of active surface sites, the turnover frequency (TOF) was calculated

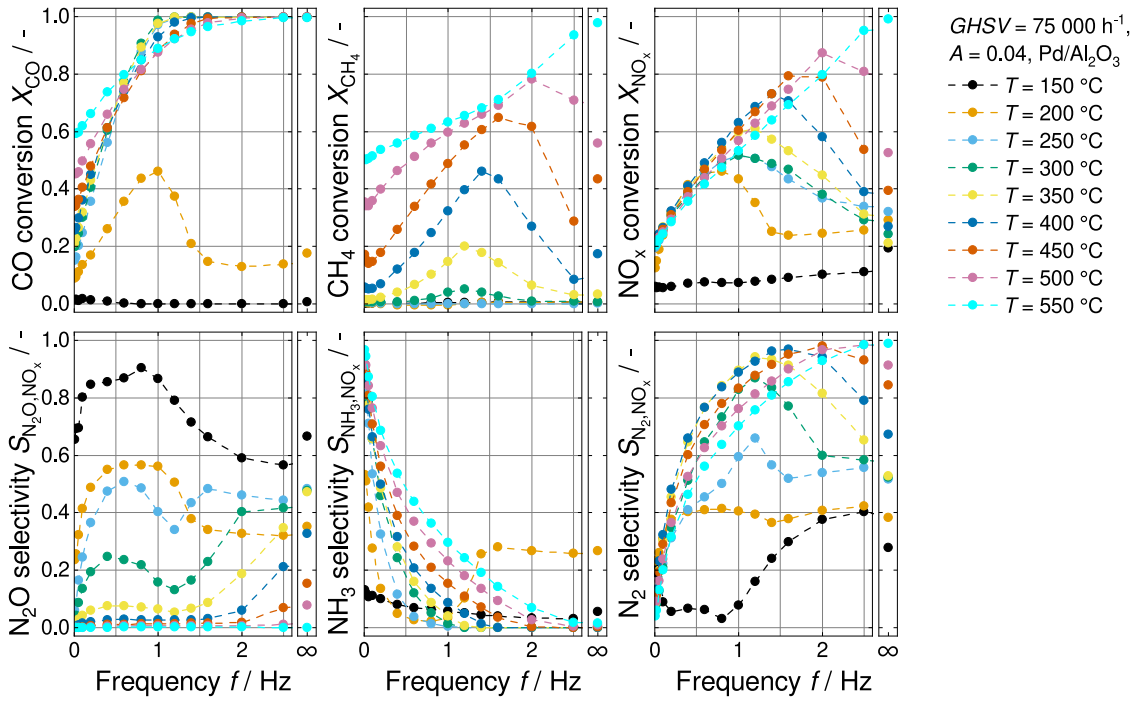

Fig. 2. Cycle-average conversion of pollutants and selectivity of products formed from NO_x at different frequencies and temperature at constant $GHSV = 75\,000\,h^{-1}$, $A = 0.04$ and stoichiometric mean λ value on Pd/Al_2O_3. The exhaust gas compositions are displayed in Fig. 1.

in accordance with Eq. (9), taking into account the dispersion of the noble metal, as measured by CO chemisorption, as well as the precious metal content determined by elemental analysis (Table S1). A dispersion of 19% and 24% was determined for Pd and Pt, respectively, by means of CO chemisorption, which corresponds to an average particle size of 5.8 nm and 4.7 nm, respectively. However, XRD patterns of Pd/Al_2O_3 and Pt/Al_2O_3 show characteristic reflections of Pt and PdO (cf. Fig. S1), which suggests a rather broad particle size distribution that also comprises some larger particles with high crystallinity.

$$TOF_i = \frac{\frac{p\dot{V}}{RT} x_{i,0} X_i}{\frac{m_{cat} x_{PGM}}{M_{PGM}} D_{PGM}} \tag{9}$$

3. Results and discussion

3.1. Temperature–frequency sweeps

Fig. 2 shows the cycle-average pollutant conversion and product selectivities derived from NO_x at different frequencies and temperatures at $GHSV = 75\,000\,h^{-1}$ and $A = 0.04$ on Pd/Al_2O_3. If not indicated otherwise, the temperature presented herein corresponds to the inlet temperature. The cycle-average pollutant conversion and product selectivities of the methane exhaust gas mixture exhibits similar behavior to the exhaust of a typical gasoline exhaust gas at stoichiometric steady-state condition and periodic conditions on the same Pd/Al_2O_3 catalyst [46]. For instance, a CO conversion of approximately 20% at 200 °C can be determined for both gas mixtures and the same operating conditions at stoichiometric steady-state conditions.

In contrast to the low light-off temperatures of C_3H_6 (T_{50} = 200–250 °C) and C_3H_8 (T_{50} = 300 °C) that were used as model hydrocarbons for the gasoline exhaust gas mixture in the past [46], CH_4, which is the only hydrocarbon in the present study, is converted at a much higher temperature (T_{50} = 450 °C) at fully-mixed stoichiometric steady-state conditions ($f \to \infty$) due to its stable tetrahedral molecular structure [2,57,58]. Moreover, the concentration of water in the exhaust gases of natural gas engines is significantly higher. This results in a strong water inhibition on Pd/Al_2O_3, causing the CH_4 light-off to further shift to higher temperatures [59,60]. Due to the stoichiometric operating conditions, full NO_x conversion is also shifted to higher temperatures reflecting its simultaneous conversion with CH_4 [37,38].

In line with the higher light-off temperature for NO_x, N_2O emissions can be observed over a wider temperature range of 150–500 °C for the methane combustion emission compared to the gasoline exhaust (150–300 °C) [46] at stoichiometric steady-state operation. Qian et al. [61] employed numerical analysis to investigate the impact of exhaust gas composition of a natural gas engine with a Pd-only TWC and showed that the partial pressures of H_2O, H_2, O_2, and CH_4 have a significant effect on the production of NH_3 and N_2O. Furthermore, the conversion of pollutants [62] and the formation of secondary emissions like N_2O and NH_3 [56] are highly sensitive to small AFR changes around $\lambda = 1$.

Compared to a fully-mixed stoichiometric steady-state operation ($f \to \infty$), CO conversion can be increased by 30% by operating the catalyst at a frequency of 1 Hz at 200 °C. At a temperature of 250 °C full CO conversion can already be achieved at the fully-mixed stoichiometric steady-state. Consequently, it is not possible to further enhance the reaction rate by operating the system periodically, as reported by Silveston [19]. However, CH_4 and NO_x conversion can be increased by up to 40% in a temperature range of 250–500 °C compared to stoichiometric steady-state conditions and the optimal frequency for maximal pollutant conversion increases from 1 Hz at 250 °C to 1.6 Hz at 400 °C. As previously reported [46], the enhanced reaction rate observed during periodic operation can be attributed to the mitigation in CO [19] and O_2 [21] poisoning of the catalyst during rich and lean conditions, respectively, by achieving an equal level of adsorbate composition on the surface [20]. Following a switch from a rich to lean or lean to rich environment, an induction period occurs during which CO or O_2 is desorbed from the noble metal surface. During the transition from a CO-poisoned surface under rich to an O-poisoned surface under lean conditions and vice versa, free surface sites become available for reactant adsorption, thereby achieving the optimal composition of adsorbates on the surface and thus the maximum reaction rate. Since the desorption of CO and O_2 is a temperature-governed process, the induction periods are shortened as the temperature increases. Consequently, the optimum surface coverage of the catalyst is reached

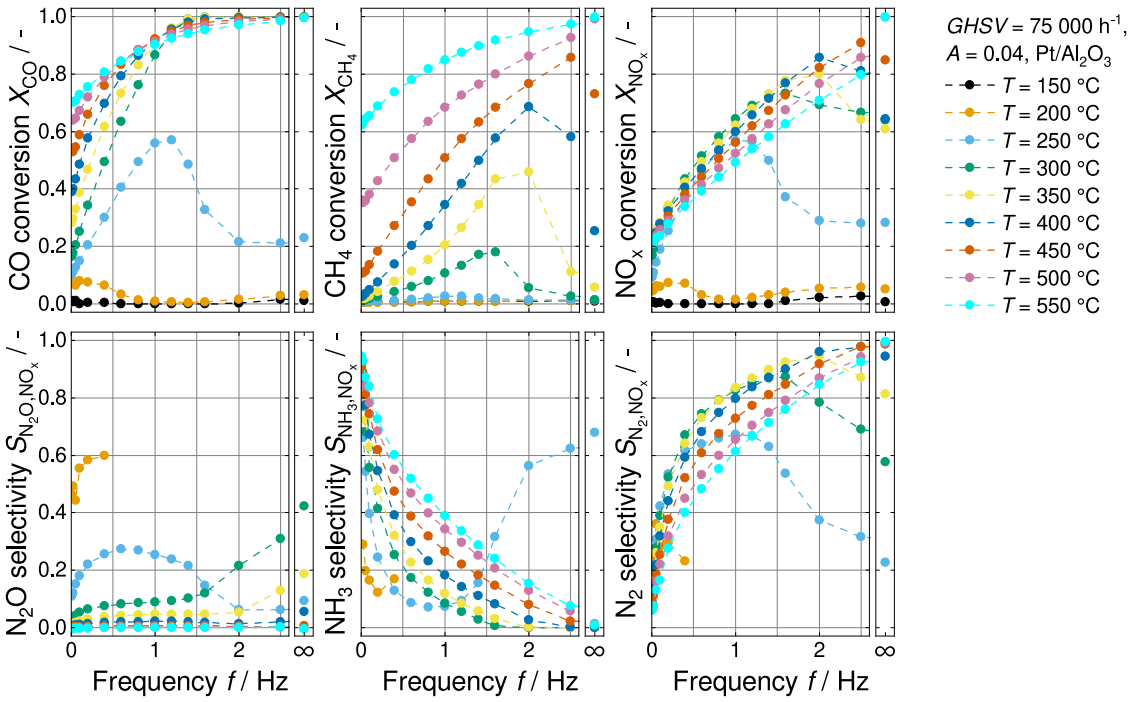

Fig. 3. Cycle-average conversion of pollutants and selectivity of products formed from NO_x at different frequencies and temperature at constant $GHSV$ = 75 000 h^{-1}, A = 0.04 and stoichiometric mean λ value on Pt/Al_2O_3. The exhaust gas compositions are displayed in Fig. 1.

more quickly after the rich-lean or lean-rich transition. A temperature-dependent induction period for CO desorption was observed after O_2 was introduced to pre-adsorbed CO on Pd/Al_2O_3 following a rich-lean switch [48]. This time lag corresponds to the minimum cycle period that is needed for rate enhancement under periodic condition [49].

Despite the identical operational parameters, including amplitude, $GHSV$, and temperature, as well as the identical catalyst, the methane exhaust gas employed in this investigation yielded higher optimal frequencies than those observed in the experiments utilizing a conventional gasoline exhaust gas mixture [46]. This can be attributed to the change in reactant concentrations. The selection of the gas mixture has a significant impact on the light-off temperatures of each exhaust gas species [63] as the catalyst is poisoned at low temperatures due to partial pressure-dependent surface coverage of the reactants [48,64]. Getsoian et al. [62] showed that the light-off temperature of propane increases with increasing CO partial pressure in the feed, which can be attributed to stronger CO inhibition on the catalytic surface. Therefore, the optimal frequency depends in particular on the CO and O_2 partial pressures during the lean and rich phases. As periodic operation reduces surface poisoning, it can be presumed that the optimal frequency is strongly dependent on the surface composition and, therefore, the applied gas mixture.

Moreover, in line with our previous study on emissions of gasoline engines, the optimal frequency for maximal pollutant conversion does not always correspond to low secondary emissions of NH_3 and N_2O, especially at temperatures as low as 150 °C and 200 °C [46]. However, maintaining an optimal frequency in a range of 250–500 °C can substantially enhance N_2 selectivity by 40% compared to fully-mixed stoichiometric steady-state conditions ($f \rightarrow \infty$).

Platinum emerges as a viable option for TWC due to its potential for higher activity in the conversion of CH_4 at stoichiometric conditions [63], as well as the fluctuation of precious metal prices [65,66]. Therefore, Fig. 3 displays the average pollutant conversion and the selectivity of secondary emissions at different frequencies and temperatures at $GHSV$ = 75 000 h^{-1} and A = 0.04 on Pt/Al_2O_3. A comparison of the TOFs at stoichiometric steady-state conditions (cf. Fig. S2) reveals that platinum exhibits a higher methane and NO_x light-off temperature and a lower CO light-off temperature compared to palladium. These findings are in agreement with those reported in the literature [63,67]. It should be noted that under stoichiometric conditions, Pd is present as a mixture of Pd and PdO_x, which assumed to reduce the activity for methane oxidation [68,69]. The higher activity for CO and NO_x conversion on Pd/Al_2O_3 at low temperatures can be attributed to a less pronounced CO inhibition on Pd [63,70].

Moreover, there is a difference in the behavior of the Pd- and Pt-based catalyst with regard to the formation of secondary emissions (cf. Fig. 3). Please note that the selectivity of the products was not depicted if the NO_x conversion was below 5% as at 150 °C and 200 °C (cf. orange line). Pt/Al_2O_3 exhibits a maximum NH_3 selectivity of 70% at 250 °C under stoichiometric steady-state conditions, while the maximum NH_3 selectivity of 30% on Pd/Al_2O_3 is observed at 200 °C, which is consistent with overall higher peak emissions of NH_3 on Pt/Al_2O_3 observed in previous studies [71,72]. The higher NH_3 emissions over Pt due to the interaction of NO, CO and H_2 can be attributed to the formation of isocyanic acid on the Pt surface and its subsequent hydrolysis in the presence of Al_2O_3 [73,74]. In agreement with the literature, Pd/Al_2O_3 shows low- and high-temperature formation of N_2O at 150 °C and 350 °C, whereas Pt/Al_2O_3 only exhibits high-temperature formation at 300 °C [10,46,71], which can be explained by the higher low temperature H_2-SCR activity of Pd compared to Pt in the presence of inhibiting CO [75,76].

Under periodic operating conditions, higher optimal frequencies are found for Pt/Al_2O_3 compared to Pd/Al_2O_3 at temperatures above 250 °C. For instance, at 350 °C, the optimal frequency for achieving maximum CH_4 conversion over the platinum-based catalyst is 1.8 Hz, whereas for the Pd/Al_2O_3 catalyst, it is approximately 1.2 Hz. A possible explanation for different optimal frequencies of the two noble metals is the different adsorption strength of CO and O_2 on Pt and Pd. In order to substantiate this hypothesis, CO-TPD measurements (Fig. S3, which presents the MS signals of CO (m/z = 28), CO_2 (m/z = 44), and H_2 (m/z = 2)) and O_2-TPD measurements (Fig. S4, which depicts the TCD signal) were conducted for Pd/Al_2O_3 and Pt/Al_2O_3, respectively. A broad CO desorption signal was observed during CO-TPD (cf. Fig. S3) for both samples between 70 °C and 350 °C, with

two desorption peaks at 100 °C and 262 °C for Pd/Al_2O_3 and at 100 °C and 240 °C for Pt/Al_2O_3, respectively. The broad CO desorption peak is a characteristic feature for Pd/Al_2O_3 [77–79] and Pt/Al_2O_3 [80–82] and can be attributed to the re-adsorption of CO [82,83]. Dropsch and Baerns [79] assigned the low-temperature peaks observed below 227 °C to the desorption of linearly bound CO, whereas the peaks observed above 227 °C were attributed to the desorption of bridge-bound CO. Moreover, the desorption of CO_2 and H_2 was observed over both catalysts during CO-TPD. Consequently, a separate measurement was conducted to exclude the presence of H_2 on the sample after reduction, which was achieved by subjecting the reduced sample to a heating process in an Ar atmosphere to a temperature of 600 °C. That during this process no desorption of H_2 was observed confirms the absence of H_2 on the sample. Instead, the desorption of CO_2 and H_2 has been previously documented and can be attributed to the Boudouard reaction and the watergas-shift reaction, with the presence of minute quantities of water in the gas bottles or OH groups on the support material [79–81,83]. As illustrated in Fig. S4, the TCD signal during O_2-TPD reveals the existence of a single O_2 desorption peak at 380 °C and 310 °C for Pd/Al_2O_3 and Pt/Al_2O_3, respectively, within the investigated temperature range, and an additional desorption peak at higher temperatures, which is in agreement with measurements on Pd(110) [84,85] and Pt(111) [86] surfaces. These findings indicate that Pd exhibits a higher binding strength for CO and O_2 in comparison to Pt, which becomes evident as well when comparing the heat of adsorption of CO [87,88] and O_2 [67,89] on Pd and Pt. Due to the weaker binding of these surface species on Pt, the desorption proceeds faster at the same temperature after a rich-lean and lean-rich switch, respectively. Therefore, higher frequencies are required to keep the catalyst in a transient state with optimal surface composition.

Another possible reason for the observed effect could be the different oxygen storage capacities of Pd and Pt. While Pd can be oxidized to PdO_x, which significantly contributes to the oxygen storage capacity (OSC) of the catalyst [90], it is reported that Pt does not form oxides under relevant TWC conditions [91,92]. Therefore, the OSCC of both catalysts, which was obtained at different temperatures during reduction of the catalyst with CO, was compared with the theoretical value for complete transition from PGM^{+II} to PGM^0 (Table 1). The total oxygen storage capacity of Pd and Pt at 550 °C is 183 µmol g^{-1} and 89 µmol g^{-1}, respectively. Since these values align closely with the theoretical values (Table 1), we can assume that the samples underwent complete reduction during the OSCC measurements conducted at 550 °C. In contrast, a comparison of the calculated values for surface oxygen with the OSCC values obtained at low temperatures indicates that there is only a reduction of surface oxygen at these temperatures. Fig. 4 displays the AFR value at the inlet and outlet of the reactor monitored by the front and rear AFR sensor at a frequency of 0.01 Hz at $GHSV = 75\,000\,h^{-1}$, $A = 0.04$ and $T = 300$ °C. It can be shown from the different slopes of the inlet (black line) and outlet (colored line) AFR data that oxygen uptake and release after a rich-lean and lean-rich switch occurs in less than one second, allowing stored oxygen to be used for the reaction during high frequency cycling. It is important to note that the presence of CO_2 and H_2O in the simulated exhaust gas significantly reduces the amount of available OSC [93]. Although a quantitative analysis of the OSC is not possible as the concentrations of H_2 and O_2 at the reactor outlet cannot be determined via FTIR measurements, a comparison of the area between the curves for the oxygen uptake and release (cf. pink area and numbers in Fig. 4) of Pd/Al_2O_3 and Pt/Al_2O_3 reveals that approximately the same amount of oxygen is released or stored for Pd/Al_2O_3 as for Pt/Al_2O_3 in the first second after the switch. Note, that the chosen frequency has an impact on the inlet and outlet AFR (cf. Fig. S5). At frequencies of 0.2 Hz and 0.4 Hz, approximately the same areas between the inlet and outlet as for the measurement at 0.01 Hz can be observed, indicating that the catalysts can rapidly utilize the stored oxygen. At higher frequencies of 0.6 Hz and 1 Hz, mixing at the inlet and along catalyst becomes

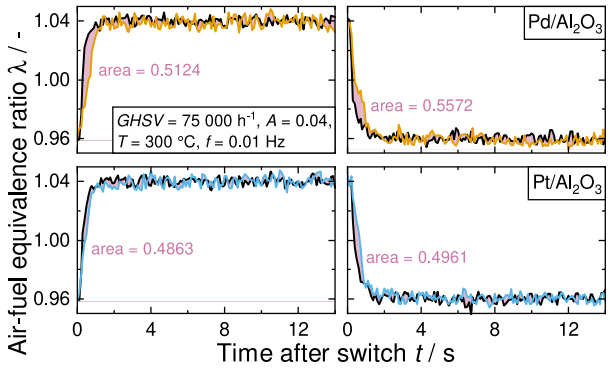

Fig. 4. Air–fuel equivalence ratio (AFR) at the inlet (black line) and outlet (colored line) of the reactor after a rich-lean switch (left) and lean-rich switch (right) for Pd/Al_2O_3 and Pt/Al_2O_3 recorded by the front and rear AFR sensors at constant $GHSV = 75\,000\,h^{-1}$, $T = 300$ °C, $A = 0.04$ and $f = 0.01$ Hz. The exhaust gas compositions are displayed in Fig. 1.

Table 1
Comparison of measured oxygen storage capacity complete (OSCC) of Pd/Al_2O_3 and Pt/Al_2O_3 at different temperatures, calculated maximal OSCC and calculated surface oxygen.

Catalysts	OSCC/µmol g^{-1} at				
	150 °C	350 °C	550 °C	Max	Surf
Pd/Al_2O_3	76	56	183	189	36
Pt/Al_2O_3	~0	23	89	92	22

relevant, which results in a dampening of the amplitude. Furthermore, the outlet AFR is dampened by the pollutant conversion that takes place during both the lean and rich phase, making it challenging to ascertain whether oxygen can be stored and released under these conditions. In order to quantify the release of oxygen, the cumulative CO_2 formation per gram of catalyst was evaluated over time during the OSCC measurements (cf. Fig. S6). The initial rates at $t = 0$ exhibited maximal CO_2 formation rates of 0.6 µmol g^{-1} s^{-1} at $T = 550$ °C for Pd/Al_2O_3 and Pt/Al_2O_3. These rates are consistent with the values reported by Descorme et al. [94] for Pd/Al_2O_3 and Pt/Al_2O_3. In light of the relatively low oxygen storage capacity and CO_2 formation rates observed for the Pd/Al_2O_3 and Pt/Al_2O_3 catalyst samples, as well as the relatively low temperature of 300 °C, it can be reasonably assumed that the observed oxygen storage and removal on the AFR sensors are indicative of the storage and removal of surface oxygen, rather than bulk oxygen. An evaluation of the AFR sensors at elevated temperatures revealed no significant increase in the area under the curve following the initial second after a switch in gas mixture. Furthermore, Ketteler et al. [95] investigated Pd(111) and observed an almost instantaneous oxidation of the Pd surface upon exposure to oxidative atmosphere. In contrast, the formation of subsurface oxygen and bulk PdO occurs within the minute timescale. These findings match the OSCC measurement data fairly well, which point to a slow reduction of the catalyst samples used herein (Fig. S6). In conclusion, the influence of the oxygen storage capacity on the optimum frequency can be considered negligible for Pd/Al_2O_3 and Pt/Al_2O_3 catalysts. Only if a component with a high OSC and high oxygen mobility is part of the catalyst formulation, the optimum frequency is affected. For CeO_2-supported Pd- and Pt catalysts, for instance, a one order of magnitude higher initial CO_2 formation rate as well as OSCC could be determined [94] compared to Al_2O_3-supported samples. With regard to dithering, previous studies [46,47] as well as results that will be discussed below in more detail (Fig. S8b) clearly prove that such high OSC results in overall lower optimum frequencies.

Fig. 5 shows the cycle-average temperature difference between inlet and outlet thermocouple at different frequencies for Pd/Al_2O_3 and Pt/Al_2O_3. The frequency at which the maximum temperature difference

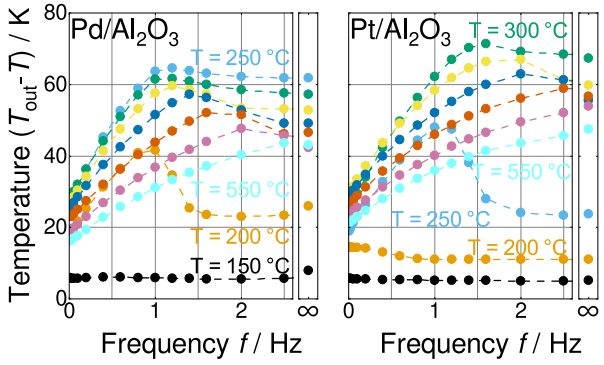

Fig. 5. Cycle-average temperature difference between outlet and inlet thermocouple at different frequencies and temperatures of (a) Pd/Al_2O_3 and (b) Pt/Al_2O_3 at constant $GHSV = 75\,000\,h^{-1}$, $A = 0.04$. The exhaust gas compositions are displayed in Fig. 1.

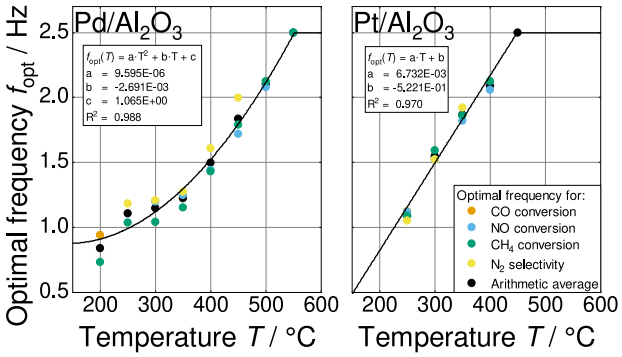

Fig. 6. Optimal frequency for maximal CO, NO, CH_4 conversion and N_2 selectivity of Pd/Al_2O_3 and Pt/Al_2O_3 at different temperatures and temperature-dependent frequency function.

is reached for Pd/Al_2O_3 at 200 °C and for Pt/Al_2O_3 at 250 °C coincides with the optimal frequency for maximum CO conversion (cf. Fig. 2 and (6)). This underscores that the increased conversion of pollutants by periodic operation is further self-amplified due to the released reaction heat and the associated heating of the catalyst [46,96]. Thus periodic operation enables rapid heating of the catalyst during cold start and therefore ensures that operating temperatures sufficient for effective pollutant conversion are reached faster. It is also notable that the maximal temperature difference decreases for temperatures above 250 °C and 300 °C for Pd/Al_2O_3 and Pt/Al_2O_3, respectively. This is attributed to the increased heat loss between the monolithic catalyst and the environment at high temperatures, as the reactor cannot be operated entirely adiabatic in the furnace. A further explanation for the higher optimal frequency of Pt under the same input conditions may therefore lie in the higher activity of Pt and the associated higher catalyst temperature due to the heat of reaction generated, which, however, also occurs in the real world application.

In summary, we conclude that the time for complete CO and O_2 desorption after a rich-lean and lean-rich switch is longer for Pd/Al_2O_3 at the same inlet temperature and that the optimal frequency is therefore at lower values compared to Pt/Al_2O_3. As dithering at lower frequencies allows simpler technical implementation due to less back-mixing, the Pd catalyst, despite its lower activity, may be considered advantageous over a Pt catalyst in terms of real-world application. Furthermore, Pd-based catalyst are particularly suitable for close-coupling to the engine due to their higher hydrothermal resistance to sintering [97,98]. However, after all also economic considerations, i.e. noble metal prices, can play a decisive role during the design of an exhaust tailpipe.

3.2. Temperature-dependent frequency control

As an alternative to a cold start under conventional stoichiometric steady-state conditions ($\lambda = 1$), Matsumoto and Shinjoh [50] suggested using the optimal frequency that enables maximum pollutant conversion at the temperature currently prevailing at the catalyst. In order to utilize the physical relationship between optimal frequency and temperature, as discussed in Section 3.1, the experimental data were fitted to polynomials. Fig. 6 illustrates the optimal frequencies for the maximum conversion of CO, NO_x and CH_4, the N_2 selectivity and their arithmetic average on Pd/Al_2O_3 and Pt/Al_2O_3 at different temperatures. The optimal frequency of the different species between the sample points was determined by fitting a Gaussian curve using three sample points and calculating the peak position of the Gaussian function. Note that the optimal frequencies of the different species determined by this method on Pd/Al_2O_3 exhibit a greater degree of variation than those on Pt/Al_2O_3. In particular, the standard deviation between the different species for Pd/Al_2O_3 is 0.1 Hz, whereas that for Pt/Al_2O_3 is 0.03 Hz. Furthermore, a second-degree polynomial fit function was employed for Pd/Al_2O_3 in order to achieve an acceptable level of agreement with the measured data.

Since these fitting parameters have no direct physical meaning and are an empirical finding, the approach chosen herein can serve as a blueprint also for entirely different conditions. For instance, even if the gas composition is changed to a gasoline engine exhaust (for conditions, see SI) and both $GHSV$ and amplitude are varied, the influence of the temperature-dependent frequency control can be captured analogously for the Pd/Al_2O_3 catalyst used herein (Fig. S7). While the optimal frequency is dependent on the specific gas mixture, it seems reasonable to assume that the same relationships for $GHSV$ and amplitude hold true for the exhaust gas of typical methane and typical gasoline engines. As the $GHSV$ and amplitude increase, the slope of the linear fit rises and the y-intercept undergoes a change that results in a shift of the optimal frequency to lower values. The literature indicates that the observed shift of the optimal frequency towards higher values with increasing amplitude [18,31,46] and $GHSV$ [45,46] at a constant temperature can be ascribed to an increase in CO and O_2 partial pressure differences between the lean and rich condition and a reduction in back-mixing in front of the catalyst, respectively. The observed increase in slope of the fit function with increasing $GHSV$ can be interpreted as an additional effect of temperature on the gas velocity (Fig. S7a). An increase in gas velocity results in a more rapid switch of the gas environment in front of the catalyst, which facilitates the desorption of adsorbates following a transition from lean to rich or rich to lean conditions and thus leads to an increase in the optimum frequency. Notably, the optimal frequency at a temperature of 150 °C is sufficiently low to render back-mixing an insignificant factor.

Since in industrial TWC formulations Pd and Pt are typically combined, a bimetallic Pd-Pt/Al_2O_3 catalyst was subject to a parameter screening as well, which allows for a direct comparison of its temperature-dependent frequency control data with the results obtained for Pd/Al_2O_3 and Pt/Al_2O_3 (cf. Fig. S8a). Despite a Pd:Pt weight-ratio of approximately 1:1 was chosen (mass fraction of Pd is 0.82% and Pt is 0.89%), the correlation between frequency and temperature obtained for Pd-Pt/Al_2O_3 falls within the error range of the results for Pd/Al_2O_3. It should be mentioned that the molar ratio of Pd to Pt on the bimetallic catalyst is approximately 63:37, which may contribute to a stronger role of Pd compared to Pt. However, this factor alone cannot explain the striking similarity between the results of Pd/Al_2O_3 and Pd-Pt/Al_2O_3. While we acknowledge that the interaction between the two noble metals can also influence the activity and desorption behavior of the bimetallic catalyst, we assume that the Pd, the noble metal with the slower desorption step regarding CO and O_2, primarily determines the dynamic process and thus the optimal frequency. Therefore, a simple interpolation between the formulas of Pd/Al_2O_3 and Pt/Al_2O_3 is an

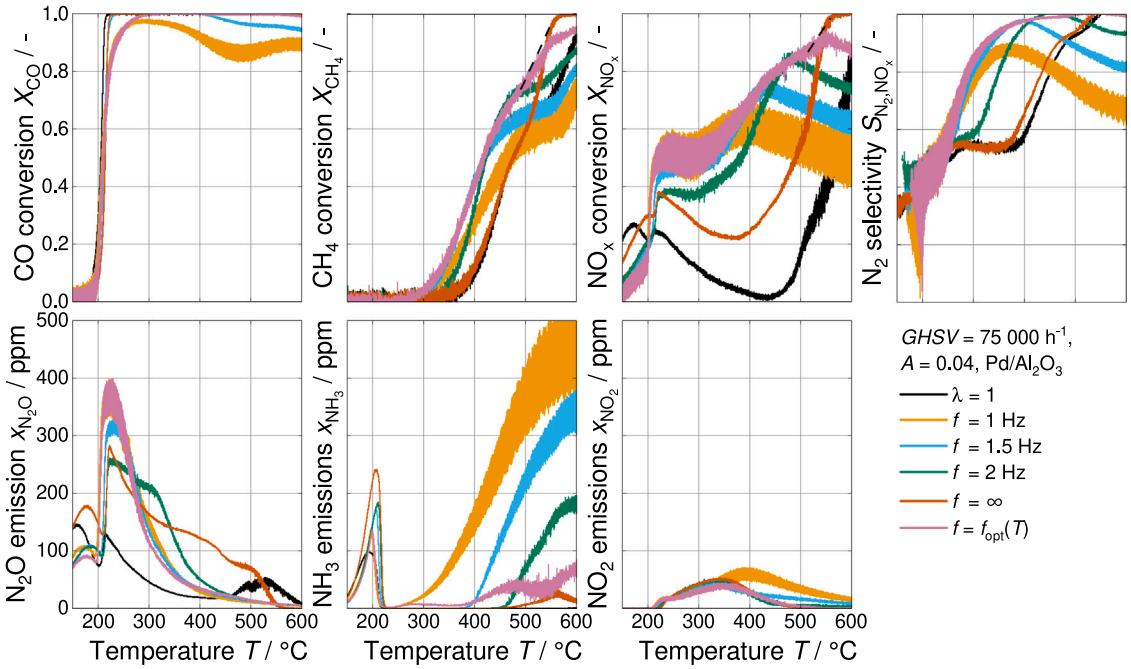

Fig. 7. Comparison of CO, CH_4, NO_x conversion, N_2 selectivity as well as N_2O, NH_3 and NO_2 emissions during light-off experiments (5 K min^{-1}) at conventional stoichiometric steady-state ($\lambda = 1$), 1 Hz, 1.5 Hz, 2 Hz, fully mixed stoichiometric steady-state ($f \rightarrow \infty$) and temperature-dependent frequency control ($f = f_{opt}(T)$) on Pd/Al_2O_3 at constant $GHSV$ = 75 000 h^{-1}, A = 0.04. The exhaust gas compositions are displayed in Fig. 1.

inadequate approach to describe the influence of temperature on optimal frequency for the bimetallic catalyst and temperature–frequency sweeps should be performed individually for every new catalyst composition. Once the correlation between frequency and temperature is known, it can directly be exploited for catalyst control in order to maximize pollutant conversion.

Furthermore, CeO_2-ZrO_2 (CZ) is commonly utilized in industrial catalyst formulations as an OSM. In order to evaluate how the oxygen storage capacity influences the temperature-dependent catalyst performance in dynamic operation, Fig. S8b compares the relationship between optimum frequency and temperature of Pd/Al_2O_3 and an industrially relevant Pd-based TWC with Y-, Nd-, and La-doped CZ that we used in a previous study for the aftertreatment of typical gasoline engine exhaust gases at $GHSV$ = 75 000 h^{-1} and A = 0.04 under periodic conditions [46]. A reduction in the optimal frequency of Pd/CZ in comparison to Pd/Al_2O_3 is evident across the entire temperature range. As previously indicated in the literature [31,46,47], increasing the OSC of the catalyst by addition of OSM decreases the optimal frequency of the catalyst. Nevertheless, an optimal frequency as a function of temperature can be derived from the kinetic data, which underscores the universality of the approach suggested in the present study: It does not only work for comparably simple catalyst formulations operated in a limited regime of conditions (herein, natural gas engine exhausts were chosen), but also works for more complex catalyst formulations operated under different conditions such as gasoline exhaust compositions.

Fig. 7 compares the CO, NO, and CH_4 conversion, N_2 selectivity, as well as the NH_3, N_2O, and NO_2 emissions during a cold start from 150 °C on Pd/Al_2O_3 with a heating ramp of 5 K min^{-1}, $GHSV$ = 75 000 h^{-1} and A = 0.04 at conventional stoichiometric steady-state ($\lambda = 1$), periodic operation at 1 Hz, 1.5 Hz, 2 Hz, fully-mixed stoichiometric steady-state ($f \rightarrow \infty$) and optimized temperature-dependent frequency control operation ($f = f_{opt}(T)$).

Conventional stoichiometric steady-state conditions exhibit faster CO light-off (T_{50} = 205 °C), slower NO_x light-off (T_{50} = 566 °C) at medium and high temperatures as well as slower CH_4 light-off at high temperatures (T_{90} = 600 °C) compared to fully-mixed steady-state conditions (T_{50} = 214 °C, T_{50} = 472 °C, T_{90} = 544 °C), which can be attributed to different stoichiometric numbers and lower partial pressure of O_2, CO and H_2 of the conventional stoichiometric mixture (cf. Fig. 1). For instance, the higher stoichiometric number ($SN = 2[O_2]/[CO]$) of the conventional stoichiometric mixture increases the reaction rate of CO oxidation due to the positive reaction order with respect to O_2 and negative reaction order with respect to CO on Pd at low temperatures [99,100]. During the light-off, two maxima in NO_x conversion are observed at low temperatures in both steady-state operating modes, whereby the temperature of the second maximum coincides with the full CO conversion, as previously observed in literature [63]. This phenomenon can be attributed to the competitive reaction of CO with the oxidizing agents NO and O_2. Similarly, the first maxima can be attributed to the competitive reaction of H_2 with NO and O_2 [56,101,102]. Furthermore, the maxima of NO_x conversion are accompanied by maxima of N_2O emissions, e.g. 180 °C and 225 °C for the fully-mixed steady-state operation, whereas a maximum of NH_3 emission at low temperature occurs between the N_2O emission maxima (205 °C). It is important to note that the higher N_2O and NH_3 emissions of the fully-mixed stoichiometric steady-state compared to the conventional stoichiometric steady-state over the entire temperature range can be attributed to the higher overall NO_x conversions. While unselective NO reduction by H_2 produces N_2O and NH_3, the reduction with CO mainly yields N_2O as secondary emission. It is conceivable that at low temperatures, N_2O is initially formed by the reduction of NO with H_2 on the Pd surface, which is largely poisoned by CO. As the temperature rises, both the desorption rate and the reaction rate of CO increase, which means that larger quantities of H_2 can be produced by the watergas-shift reaction, which might explain the delay of NH_3 emissions [61,103]. The second N_2O maximum correlates with full CO conversion [10]. Moreover, the emission of NO_2 increases as soon as complete conversion of CO is achieved. This indicates that the catalyst surface undergoes a change from a predominantly CO-covered surface to a predominantly O-covered surface. The maximal NO_2 emissions under stoichiometric steady-state conditions can be observed at 350 °C, where O_2 desorption begins to become significant [104,105]. High-temperature NH_3 emissions correspond to full CH_4 conversion and can be attributed to steam reforming processes [37,39].

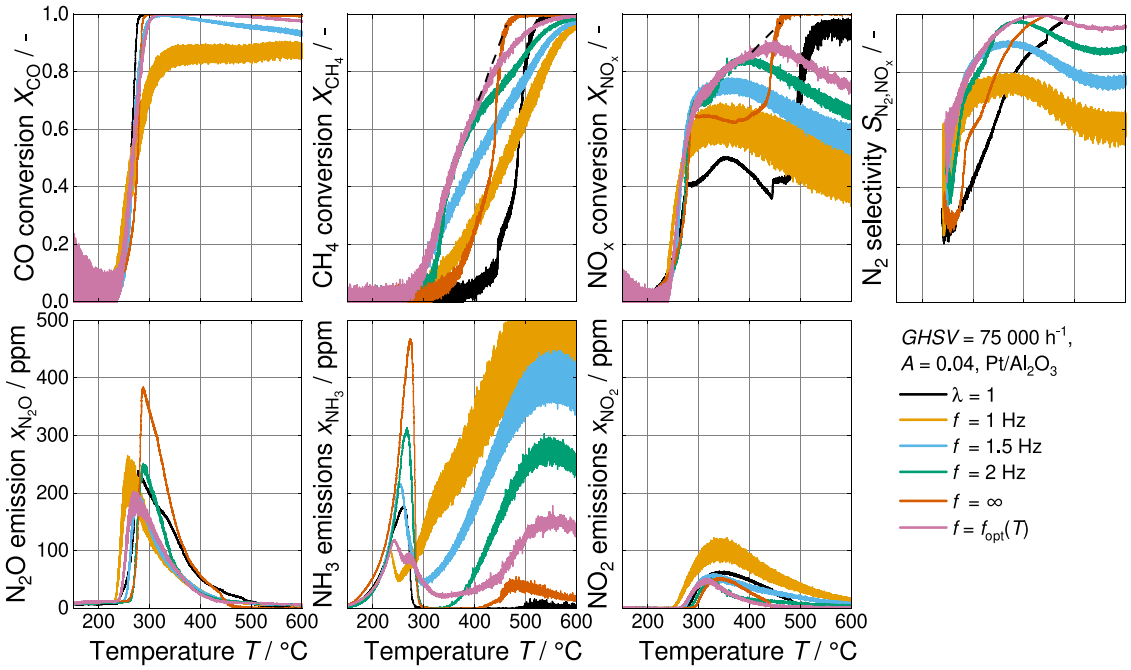

Fig. 8. Comparison of CO, CH_4, NO_x conversion, N_2 selectivity as well as N_2O, NH_3 and NO_2 emissions during light-off experiments (5 K min^{-1}) at conventional stoichiometric steady-state ($\lambda = 1$), 1 Hz, 1.5 Hz, 2 Hz, fully mixed stoichiometric steady-state ($f \rightarrow \infty$) and temperature-dependent frequency control ($f = f_{opt}(T)$) on Pt/Al_2O_3 at constant $GHSV$ = 75 000 h^{-1}, A = 0.04. The exhaust gas compositions are displayed in Fig. 1.

At constant frequencies of 1 Hz, 1.5 Hz, and 2 Hz the NO_x conversion can be increased in a temperature range of 200–500 °C, 210–520 °C and 230–530 °C and the CH_4 conversion can be increased up to a maximum temperature of 500 °C, 520 °C, 530 °C compared to the fully-mixed stoichiometric steady-state. This is consistent with gasoline engine test bench measurements on Pt/Al_2O_3, which demonstrate higher CO and HC conversions up to a temperature of 300 °C at 0.1 Hz compared to steady operation under slightly lean average AFR [24]. Analogously, Pt-Pd/Al_2O_3 show higher NO_x and CH_4 conversion up to 420 °C using synthetic exhaust gas with methane at frequency of 1 Hz [39]. This phenomenon has also been observed in the oxidation of CO on Pt/Al_2O_3 [23] and Pd/Al_2O_3 [50]. Cho [22] reported that at low temperature, periodic operation improves the conversion by perturbing the biased reactant distribution on the surface that would otherwise prevail under steady operating conditions. Conversely, at high temperatures, periodic operation impairs the conversion by perturbation of the evenly distributed reactants on the surface prevailing under steady operating conditions.

As the desorption rate increases with increasing temperature, higher frequencies are required to maintain an even distribution of the catalyst surface and thus maximize pollutant conversion [19]. Therefore, controlling the frequency of lean-rich switches with the inlet temperature can result in enhanced light-off performance on the catalyst compared to conventional stoichiometric steady-state mode. For instance, the entire CH_4 light-off curve can be shifted by approximately 60 °C to lower temperatures. While the NO_x conversion is lower at low temperatures during periodic operation due to the rapid CO light-off under conventional stoichiometric steady-state conditions, optimized dynamic operation ($f = f_{opt}(T)$) benefits the NO_x light-off significantly, which becomes particularly relevant at a temperature of 200 °C and above. 50% NO_x conversion can be achieved at 225 °C compared to 560 °C under conventional stoichiometric conditions. At temperatures above 550 °C, CH_4 and NO_x conversion are reduced compared to the fully-mixed stoichiometric steady-state. This can be attributed to the restriction of the switching valves of the experimental setup to operate beyond the maximal frequency of 2.5 Hz, which is necessary to achieve complete phase mixing in front of the catalyst in order to reach the fully-mixed stoichiometric steady-state. At higher frequencies, periodic operation is superseded by the fully-mixed stoichiometric steady-state operation [18,31,46], as indicated by the dashed lines at 550 °C in Fig. 7.

The higher N_2O and NH_3 emissions at low temperatures during periodic operation with fixed frequencies of 1 Hz, 1.5 Hz, and 2 Hz can be primarily attributed to the higher NO_x conversions compared to the conventional stoichiometric steady-state operation. On the other hand, high-temperature NH_3 and NO_2 emission during periodic operation can be attributed to enhanced steam reforming under prolonged rich and enhanced NO oxidation under prolonged lean conditions [39,40,46]. Strong NH_3 slip can be significantly reduced when an optimized temperature-dependent frequency control is employed, whereby the frequency is controlled with respect to temperature, in comparison to periodic operation at a constant frequency. Furthermore, the overall cycle-average N_2 selectivity can be increased compared to the conventional stoichiometric steady-state operation.

As underscored by the data shown in Fig. 8, namely a comparison of the conversion of CO, NO, and CH_4, as well as the selectivity of N_2, and the emissions of NH_3, N_2O, and NO_2 during a cold start from 150 °C on Pt/Al_2O_3 with a heating ramp of 5 K min^{-1}, GHSV = 75 000 h^{-1}, and A = 0.04, the same approach can be used for maximizing pollutant conversion over Pt-based catalysts. The results were obtained at conventional stoichiometric steady-state ($\lambda = 1$), periodic operation at 1 Hz, 1.5 Hz, 2 Hz, fully-mixed stoichiometric steady-state ($f \rightarrow \infty$), and optimized temperature-dependent frequency control operation ($f = f_{opt}(T)$).

In agreement with the experiments at constant temperatures, Pt/Al_2O_3 exhibits a lower CO and NO_x conversion activity at low temperatures compared to Pd/Al_2O_3, which is evident by a higher light-off temperature in all operating modes. Furthermore, only one N_2O peak emission is observed that correlates with the CO light-off temperature, which is why it can be assumed that CO and H_2 are converted at the same temperature if Pt is used as active species. Furthermore, the CH_4 and NO_x light-offs are shifted to lower light-off temperatures compared to Pd/Al_2O_3. It is noteworthy that CH_4 and NO_x exhibit a reproducible sudden increase in the conversion at 450 °C

in conventional stoichiometric steady-state mode. This phenomenon may be attributed to steady-state multiplicity of methane conversion at sub-stoichiometric conditions, where at low oxygen concentrations, there is a high conversion regime, while at high oxygen concentrations, there is a low conversion regime due to oxygen inhibition [106]. Consistent with the results on Pd/Al_2O_3, the periodic operation of Pt/Al_2O_3 increases the CH_4 and NO_x conversion as well as the N_2 selectivity in a temperature range which increases with increasing frequency compared to the conventional stoichiometric steady-state operation. Catalyst operation at the optimal temperature-controlled frequency enables a reduction in the CH_4 light-off temperature from T_{50} = 485 °C to T_{50} = 365 °C and the NO_x light-off temperature from T_{50} = 485 °C to T_{50} = 270 °C. In agreement with Muraki et al. [18] Pt/Al_2O_3 exhibits the higher rate enhancement for hydrocarbon conversion when applying periodic operation, which might be attributed to a stronger blockage of Pt surface sites.

4. Conclusion

This study introduces a novel temperature-dependent frequency control technique aimed at enhancing pollutant emission reduction and N_2 selectivity for Pd/Al_2O_3 and Pt/Al_2O_3 model three-way catalysts for controlling emissions form natural gas engines operated under stoichiometric conditions.

To determine the most effective frequency for these catalysts relative to temperature, temperature–frequency sweep experiments were conducted. Results indicate that the optimal frequency for Pt/Al_2O_3 exceeds that found for Pd/Al_2O_3 at the same temperature. This difference may be attributed to the higher oxygen storage capacity (OSC), stronger binding of inhibiting surface species CO and O and lower exothermicity due to lower activity of Pd/Al_2O_3. The CO and O_2-TPD experiments yielded evidence that O_2 and CO exhibited stronger binding on Pd, while the impact of OSC could be deemed insignificant due to the limited capacity and initial rates of oxygen release observed in this study. As the desorption rate of the inhibiting surface species increases with increasing temperature after a rich-lean and lean-rich switch, respectively, higher frequencies are required to maintain the catalyst in a transient state with optimal surface composition.

Utilizing the collected data, a temperature-dependent function for the optimal frequency was derived. This function was then tested in light-off experiments and compared against fixed frequencies of 1 Hz, 1.5 Hz, and 2 Hz, as well as conventional stoichiometric steady-state operation. It was found that fixed-frequency operation only improved pollutant conversion within a specific temperature range, with substantial formation of undesired NH_3 observed at elevated temperatures. Conversely, the temperature-dependent frequency approach significantly enhanced CH_4 and NO_x light-off temperatures by 120 K and 210 K on Pt/Al_2O_3, and by 60 K and 335 K on Pd/Al_2O_3, respectively, while also improving N_2 selectivity. Consequently, the increased low-temperature activity may reduce the need for higher catalyst loading and thus decrease the demand for scarce and expensive noble metals.

This study serves as a blueprint and proposes a cost-effective and simple method for optimizing three-way catalyst operation during cold starts without altering engine settings. The integration of a thermocouple within the catalyst enables the establishment of a relationship between optimal frequency and catalyst temperature, which can then be utilized for frequency control during cold engine starts. In conclusion, the study highlights the potential of lambda-dithering in enhancing emission control efficiency for natural gas engines as commonly applied in vehicles and mobile applications, offering valuable insights for the development and operation of catalysts tailored for cleaner urban driving environments.

CRediT authorship contribution statement

Daniel Hodonj: Writing – original draft, Visualization, Validation, Project administration, Methodology, Investigation, Formal analysis, Data curation, Conceptualization. **Barbara Thiele:** Writing – review & editing, Investigation, Formal analysis. **Olaf Deutschmann:** Writing – review & editing, Supervision, Resources, Project administration, Funding acquisition, Conceptualization. **Patrick Lott:** Writing – review & editing, Validation, Supervision, Project administration, Methodology, Funding acquisition, Data curation, Conceptualization.

Declaration of competing interest

The authors declare that they have no known competing financial interests or personal relationships that could have appeared to influence the work reported in this paper.

Data availability

Data will be made available on request.

Acknowledgments

The authors acknowledge T. Bergfeldt (IAM, KIT) for elemental analysis, T. Eldridge and K. Elfner (both ITCP, KIT) for BET, L. Braun (ITCP, KIT) for XRD, K. Schäfer and L. Almeida de Campos (both ITCP, KIT) for TPD. We would like to thank M. Casapu, A. De Giacinto (both ITCP, KIT), S. Tischer (IKFT, KIT), J. Kusaka (NextGV, Waseda University) for fruitful discussions and Sasol for providing alumina support material. This work was funded by the Deutsche Forschungsgemeinschaft (DFG, German Research Foundation) – SFB 1441 – Project-ID 426888090 and the German Federal Ministry for Economic Affairs and Climate Action (BMWK) Project-ID 314 EN.

Appendix A. Supplementary data

Supplementary material related to this article can be found online at https://doi.org/10.1016/j.cej.2024.155852.

References

[1] R. Schlögl, E-mobility and the energy transition, Angew. Chem. Int. Edn 56 (37) (2017) 11019–11022, http://dx.doi.org/10.1002/anie.201701633.
[2] M. Wang, P. Dimopoulos Eggenschwiler, T. Franken, D. Ferri, O. Kröcher, Reaction pathways of methane abatement in Pd-Rh three-way catalyst in heavy duty applications: A combined approach based on exhaust analysis, model gas reactor and DRIFTS measurements, Chem. Eng. J. 422 (2021) 129932, http://dx.doi.org/10.1016/j.cej.2021.129932.
[3] S. Verhelst, P. Maesschalck, N. Rombaut, R. Sierens, Increasing the power output of hydrogen internal combustion engines by means of supercharging and exhaust gas recirculation, Int. J. Hydrog. Energy 34 (10) (2009) 4406–4412, http://dx.doi.org/10.1016/j.ijhydene.2009.03.037.
[4] M. Berckmüller, H. Rottengruber, A. Eder, N. Brehm, G. Elsässer, G. Müller-Alander, C. Schwarz, Potentials of a charged SI-hydrogen engine, SAE Tech. Pap. 2003-10-27 (2003) http://dx.doi.org/10.4271/2003-01-3210.
[5] O. Deutschmann, J.-D. Grunwaldt, Abgasnachbehandlung in mobilen Systemen: Stand der Technik, Herausforderungen und Perspektiven, Chem. Ing. Tech. 85 (5) (2013) 595–617, http://dx.doi.org/10.1002/cite.201200188.
[6] P. Lott, O. Deutschmann, Lean-burn natural gas engines: Challenges and concepts for an efficient exhaust gas aftertreatment system, Emiss. Control Sci. Technol. 7 (1) (2021) 1–6, http://dx.doi.org/10.1007/s40825-020-00176-w.
[7] P. Lott, M. Casapu, J.-D. Grunwaldt, O. Deutschmann, A review on exhaust gas after-treatment of lean-burn natural gas engines – From fundamentals to application, Appl. Catal. B 340 (2024) 123241, http://dx.doi.org/10.1016/j.apcatb.2023.123241.
[8] O. Boucher, P. Friedlingstein, B. Collins, K.P. Shine, The indirect global warming potential and global temperature change potential due to methane oxidation, Environ. Res. Lett. 4 (4) (2009) 044007, http://dx.doi.org/10.1088/1748-9326/4/4/044007.

[9] T. Huai, T.D. Durbin, S.H. Rhee, J.M. Norbeck, Investigation of emission rates of ammonia, nitrous oxide and other exhaust compounds from alternativefuel vehicles using a chassis dynamometer, Int. J. Automot. Technol. 4 (1) (2003) 9–19.

[10] I. Mejía-Centeno, S. Castillo, G.A. Fuentes, Enhanced emissions of NH_3, N_2O and H_2 from a Pd-only TWC and supported Pd model catalysts: Light-off and sulfur level studies, Appl. Catal. B 119–120 (2012) 234–240, http://dx.doi.org/10.1016/j.apcatb.2012.02.030.

[11] S.K. Hoekman, Review of nitrous oxide (N_2O) emissions from motor vehicles, SAE Int. J. Fuels Lubr. 13 (1) (2020) 79–98, http://dx.doi.org/10.4271/04-13-01-0005.

[12] J. Sun, A.J. Barnes, D. He, M. Wang, J. Wang, Systematic review and meta-analysis of the association between ambient nitrogen dioxide and respiratory disease in China, Int. J. Environ. Res. Public Health 14 (6) (2017) 646, http://dx.doi.org/10.3390/ijerph14060646.

[13] B. Ge, X. Xu, Z. Ma, X. Pan, Z. Wang, W. Lin, B. Ouyang, D. Xu, J. Lee, M. Zheng, Role of ammonia on the feedback between AWC and inorganic aerosol formation during heavy pollution in the North China Plain, Earth Space Sci. 6 (9) (2019) 1675–1693, http://dx.doi.org/10.1029/2019EA000799.

[14] M.V. Prati, M.A. Costagliola, A. Unich, A. Mariani, Emission factors and fuel consumption of CNG buses in real driving conditions, Transp. Res. D 113 (2022) 103534, http://dx.doi.org/10.1016/j.trd.2022.103534.

[15] T. Okajima, S. Sivakumar, H. Shingyouchi, K. Yamaguchi, J. Kusaka, M. Nagata, Modeling on a three-way catalyst used in series hybrid electric vehicles considering its specific engine operation attribute, Ind. Eng. Chem. Res. 60 (4) (2021) 1583–1601, http://dx.doi.org/10.1021/acs.iecr.0c05436.

[16] L. Ntziachristos, G. Papadopoulos, Z. Samos, N. Tsalikidis, G. Mellios, A. Dimaratos, A. Kontses, D. Kontses, Z. Samaras, Euro 7 Impact Assessment Study, Publications Office of the European Union Europäische Kommission, Luxembourg, 2022, http://dx.doi.org/10.2873/249061.

[17] P.L. Silveston, R.R. Hudgins, Combustion systems, in: P. Silveston, R. Hudgins (Eds.), Periodic Operation of Chemical Reactors, Butterworth-Heinemann, Oxford, 2013, pp. 123–140, http://dx.doi.org/10.1016/B978-0-12-391854-3.00005-X.

[18] H. Muraki, H. Shinjoh, H. Sobukawa, K. Yokota, Y. Fujitani, Behavior of automotive noble metal catalysts in cycled feedstreams, Ind. Eng. Chem. Res. 24 (1) (1985) 43–49, http://dx.doi.org/10.1021/i300017a009.

[19] P.L. Silveston, Automotive exhaust catalysis: Is periodic operation beneficial? Chem. Engi. Sci. 51 (10) (1996) 2419–2426, http://dx.doi.org/10.1016/0009-2509(96)00098-x.

[20] M.B. Cutlip, Concentration forcing of catalytic surface rate processes: Part I. Isothermal carbon monoxide oxidation over supported platinum, AIChE J. 25 (3) (1979) 502–508, http://dx.doi.org/10.1002/aic.690250316.

[21] P.-A. Carlsson, S. Mollner, K. Arnby, M. Skoglundh, Effect of periodic operation on the low-temperature activity for propane oxidation over Pt/Al_2O_3 catalysts, Chem. Eng. Sci. 59 (20) (2004) 4313–4323, http://dx.doi.org/10.1016/j.ces.2004.06.024.

[22] B.K. Cho, Dynamic behavior of a single catalyst pellet 1. Symmetric concentration cycling during carbon monoxide oxidation over platinum/alumina, Ind. Eng. Chem. Fund. 22 (4) (1983) 410–420, http://dx.doi.org/10.1021/i100012a010.

[23] B.K. Cho, L.A. West, Cyclic operation of platinum/alumina catalysts for carbon monoxide oxidation, Ind. Eng. Chem. Fund. 25 (1) (1986) 158–164, http://dx.doi.org/10.1021/i100021a025.

[24] B.K. Cho, Performance of platinum/alumina catalysts in automobile engine exhaust with oscillatory air/fuel ratio, Ind. Eng. Chem. Res. 27 (1) (1988) 30–36, http://dx.doi.org/10.1021/ie00073a007.

[25] M. Roger, O. Kröcher, D. Ferri, Assessing the effect of O_2 dithering on CH_4 oxidation on Pd/Al_2O_3, Chem. Eng. J. 451 (2023) 138865, http://dx.doi.org/10.1016/j.cej.2022.138865.

[26] X. Shi, R. Seiser, J.-Y. Chen, R. Dibble, R. Cattolica, Fuel-dithering optimization of efficiency of TWC on natural gas IC engine, SAE Int. J. Engines 8 (3) (2015) 1246–1252, http://dx.doi.org/10.4271/2015-01-1043.

[27] J. Gong, J. Pihl, D. Wang, M.-Y. Kim, W.P. Partridge, J. Li, M. Cunningham, K. Kamasamudram, N. Currier, A. Yezerets, O_2 dosage as a descriptor of TWC performance under lean/rich dithering in stoichiometric natural gas engines, Catal. Today 360 (01) (2021) 294–304, http://dx.doi.org/10.1016/j.cattod.2020.02.022.

[28] F. Zeng, J. Finke, D. Olsen, A. White, K.L. Hohn, Modeling of three-way catalytic converter performance with exhaust mixtures from dithering natural gas-fueled engines, Chem. Eng. J. 352 (2018) 389–404, http://dx.doi.org/10.1016/j.cej.2018.07.005.

[29] L. Hegedus, Poison-resistant catalysts for the simultaneous control of hydrocarbon, carbon monoxide, and nitrogen oxide emissions, J. Catal. 56 (3) (1979) 321–335, http://dx.doi.org/10.1016/0021-9517(79)90125-8.

[30] J.C. Schlatter, R.M. Sinkevitch, P.J. Mitchell, Laboratory reactor system for three-way automotive catalyst evaluation, Ind. Eng. Chem. Res. 22 (1) (1983) 51–56, http://dx.doi.org/10.1021/i300009a013.

[31] L. Padeste, A. Baiker, Three-way catalysts in a hybrid drive system: 1. Experimental study of dynamic behavior, Ind. Eng. Chem. Res. 33 (5) (1994) 1113–1119, http://dx.doi.org/10.1021/ie00029a007.

[32] F. Klingstedt, A.K. Neyestanaki, R. Byggningsbacka, L.-E. Lindfors, M. Lundén, M. Petersson, P. Tengström, T. Ollonqvist, J. Väyrynen, Palladium based catalysts for exhaust aftertreatment of natural gas powered vehicles and biofuel combustion, Appl. Catal. A: Gen. 209 (1–2) (2001) 301–316, http://dx.doi.org/10.1016/S0926-860X(00)00768-7.

[33] D. Bounechada, G. Groppi, P. Forzatti, K. Kallinen, T. Kinnunen, Effect of periodic lean/rich switch on methane conversion over a Ce–Zr promoted $Pd-Rh/Al_2O_3$ catalyst in the exhausts of natural gas vehicles, Appl. Catal. B 119–120 (2012) 91–99, http://dx.doi.org/10.1016/j.apcatb.2012.02.025.

[34] D. Bounechada, G. Groppi, P. Forzatti, K. Kallinen, T. Kinnunen, Enhanced methane conversion under periodic operation over a Pd/Rh based TWC in the exhausts from NGVs, Top. Catal. 56 (1–8) (2013) 372–377, http://dx.doi.org/10.1007/s11244-013-9982-8.

[35] S. Fouladvand, M. Skoglundh, P.-A. Carlsson, Unsteady-state operation of supported platinum catalysts for high conversion of methane, Chem. Eng. J. 292 (2016) 321–325, http://dx.doi.org/10.1016/j.cej.2016.02.033.

[36] D. Karamitros, A. Ibraimova, K. Konstantinidis, G. Koltsakis, S. Choi, J. Cho, Methane conversion in stoichiometric natural gas engine exhaust, SAE Tech. Pap. 2024-01-2632 (2024) http://dx.doi.org/10.4271/2024-01-2632.

[37] D. Ferri, M. Elsener, O. Kröcher, Methane oxidation over a honeycomb pd-only three-way catalyst under static and periodic operation, Appl. Catal. B 220 (2018) 67–77, http://dx.doi.org/10.1016/j.apcatb.2017.07.070.

[38] S.B. Kang, K. Karinshak, P.W. Chen, S. Golden, M.P. Harold, Coupled methane and NOx conversion on Pt + Pd/Al_2O_3 monolith: Conversion enhancement through feed modulation and $Mn_{0.5}Fe_{2.5}O_4$ spinel addition, Catal. Today 360 (2021) 284–293, http://dx.doi.org/10.1016/j.cattod.2020.02.039.

[39] K. Karinshak, P.W. Chen, R.-F. Liu, S.J. Golden, M.P. Harold, Optimizing feed modulation for coupled methane and NOx conversion over $Pd-Pt/Mn_{0.5}Fe_{2.5}O_4/Al_2O_3$ monolith catalyst, Appl. Catal. B 304 (2022) 120607, http://dx.doi.org/10.1016/j.apcatb.2021.120607.

[40] M. Wang, P. Dimopoulos Eggenschwiler, D. Ferri, O. Kröcher, Experimental and modeling-based analysis of reaction pathways on catalysts for natural gas engines under periodic lean/rich oscillations, Chem. Eng. J. 430 (10) (2022) 132848, http://dx.doi.org/10.1016/j.cej.2021.132848.

[41] R.H. Hammerle, C.H. Wu, Effect of high temperatures on three-way automotive catalysts, SAE Tech. Pap. 1984-02-01 (1984) http://dx.doi.org/10.4271/840549.

[42] J. Kašpar, P. Fornasiero, N. Hickey, Automotive catalytic converters: current status and some perspectives, Catal. Today 77 (4) (2003) 419–449, http://dx.doi.org/10.1016/S0920-5861(02)00384-X.

[43] K. Yokota, H. Muraki, Y. Fujitani, Rh-free three-way catalysts for automotive exhaust control, SAE Tech. Pap. 1985-02-01 (1985) http://dx.doi.org/10.4271/850129.

[44] J.C. Summers, L.L. Hegedus, Modes of catalyst deactivation in stoichiometric automobile exhaust, Ind. Eng. Chem. Prod. Res. Dev. 18 (4) (1979) 318–324, http://dx.doi.org/10.1021/i360072a018.

[45] A. Reihani, G.B. Fisher, J.W. Hoard, J.R. Theis, J.D. Pakko, C.K. Lambert, Rapidly pulsed reductants for diesel NOx reduction with lean NOx traps: Effects of pulsing parameters on performance, Appl. Catal. B 223 (2018) 177–191, http://dx.doi.org/10.1016/j.apcatb.2017.07.054.

[46] D. Hodonj, M. Borchers, L. Zeh, G.T. Hoang, S. Tischer, P. Lott, O. Deutschmann, Impact of operation parameters and lambda input signal during lambda-dithering of three-way catalysts for low-temperature performance enhancement, Appl. Catal. B 345 (2024) 123657, http://dx.doi.org/10.1016/j.apcatb.2023.123657.

[47] T. Nakase, T. Hattori, J. Naito, K. Kondo, Method of operating a three-way catalyst for internal combustion, 1980, Patent No. US4199938A.

[48] Y. Barshad, E. Gulari, A novel catalytic reactor system for transient response and its use in CO oxidation on Pd/Al_2O_3, J. Catal. 94 (2) (1985) 468–477, http://dx.doi.org/10.1016/0021-9517(85)90211-8.

[49] X. Zhou, Y. Barshad, E. Gulari, Co oxidation on Pd/Al_2O_3. Transient response and rate enhancement through forced concentration cycling, Chem. Eng. Sci. 41 (5) (1986) 1277–1284, http://dx.doi.org/10.1016/0009-2509(86)87100-7.

[50] S. Matsumoto, H. Shinjoh, Dynamic behavior and characterization of automobile catalysts, in: G.B. Marin (Ed.), Automotive Emission Control, in: Advances in Chemical Engineering, vol. 33, Academic Press, 2007, pp. 1–46, http://dx.doi.org/10.1016/S0065-2377(07)33001-9.

[51] K.A. Karinshak, P. Lott, M.P. Harold, O. Deutschmann, In situ activation of bimetallic Pd−Pt methane oxidation catalysts, ChemCatChem 12 (14) (2020) 3712–3720, http://dx.doi.org/10.1002/cctc.202000603.

[52] K.G. Rappé, C. DiMaggio, J.A. Pihl, J.R. Theis, S.H. Oh, G.B. Fisher, J. Parks, V.G. Easterling, M. Yang, M.L. Stewart, K.C. Howden, Aftertreatment protocols for catalyst characterization and performance evaluation: Low-temperature oxidation, storage, three-way, and NH_3-SCR catalyst test protocols, Emiss. Control Sci. Technol. 5 (2) (2019) 183–214, http://dx.doi.org/10.1007/s40825-019-00120-7.

[53] S. Brunauer, P.H. Emmett, E. Teller, Adsorption of gases in multimolecular layers, J. Am. Chem. Soc. 60 (2) (1938) 309–319, http://dx.doi.org/10.1021/ja01269a023.

[54] C. Karakaya, O. Deutschmann, A simple method for CO chemisorption studies under continuous flow: Adsorption and desorption behavior of Pt/Al_2o_3 catalysts, Appl. Catal. A: Gen. 445–446 (2012) 221–230, http://dx.doi.org/10.1016/j.apcata.2012.08.022.

[55] G. Bergeret, P. Gallezot, Particle Size and Dispersion Measurements, in: G. Ertl, H. Knözinger, F. Schüth, J. Weitkamp (Eds.), Handbook of Heterogeneous Catalysis, Vol. 7, Wiley-VCH Verlag GmbH & Co. KGaA, Weinheim, 2008, pp. 738–765, http://dx.doi.org/10.1002/9783527610044.hetcat0038.

[56] C. Wang, W. Xia, D. Yang, T. Zheng, Y. Rong, J. Du, B. Wu, Y. Zhao, Understanding ammonia and nitrous oxide formation in typical three-way catalysis during the catalyst warm-up period, J. Hazard. Mater. 438 (2022) 129553, http://dx.doi.org/10.1016/j.jhazmat.2022.129553.

[57] A. Raj, Methane emission control, Johnson Matthey Technol. Rev. 60 (4) (2016) 228–235, http://dx.doi.org/10.1595/205651316X692554.

[58] T. Bäroth, A. Drochner, H. Vogel, M. Votsmeier, Effect of diverse hydrocarbons on the cold start behavior of three-way catalysts, Top. Catal. 60 (2017) 278–282, http://dx.doi.org/10.1007/s11244-016-0609-8.

[59] P. Velin, M. Ek, M. Skoglundh, A. Schaefer, A. Raj, D. Thompsett, G. Smedler, P.-A. Carlsson, Water Inhibition in Methane Oxidation over Alumina Supported Palladium Catalysts, J. Phys. Chem. C 123 (42) (2019) 25724–25737, http://dx.doi.org/10.1021/acs.jpcc.9b07606.

[60] K. Keller, P. Lott, H. Stotz, L. Maier, O. Deutschmann, Microkinetic modeling of the oxidation of methane over PdO catalysts—Towards a better understanding of the water inhibition effect, Catalysts 10 (8) (2020) http://dx.doi.org/10.3390/catal10080922.

[61] Y. Qian, X. Wei, Y. Sun, F. Tang, S. Meng, L. Qiu, T. Wang, B. Ye, T. Pan, Y. Zhang, Investigation of the formation characteristics of N_2O and NH_3 for stoichiometric natural gas engines with Pd-only catalyst, Fuel 329 (2022) 125223, http://dx.doi.org/10.1016/j.fuel.2022.125223.

[62] A.B. Getsoian, J.R. Theis, C.K. Lambert, Sensitivity of three-way catalyst light-off temperature to air-fuel ratio, Emiss. Control Sci. Technol. 4 (3) (2018) 136–142, http://dx.doi.org/10.1007/s40825-018-0089-3.

[63] A. Gremminger, J. Pihl, M. Casapu, J.-D. Grunwaldt, T.J. Toops, O. Deutschmann, PGM based catalysts for exhaust-gas after-treatment under typical diesel, gasoline and gas engine conditions with focus on methane and formaldehyde oxidation, Appl. Catal. B 265 (2020) 118571, http://dx.doi.org/10.1016/j.apcatb.2019.118571.

[64] B. Banse, Transient kinetic studies of the catalytic reduction of NO by CO on platinum, J. Catal. 119 (1) (1989) 238–248, http://dx.doi.org/10.1016/0021-9517(89)90149-8.

[65] J. Zhang, M.P. Everson, T.J. Wallington, F.R. Field III, R. Roth, R.E. Kirchain, Assessing economic modulation of future critical materials use: the case of automotive-related platinum group metals, Environ. Sci. Tech. 50 (14) (2016) 7687–7695, http://dx.doi.org/10.1021/acs.est.5b04654.

[66] D. Bao, Dynamics and correlation of platinum-group metals spot prices, Resour. Policy 68 (2020) 101772, http://dx.doi.org/10.1016/j.resourpol.2020.101772.

[67] R. Burch, P.K. Loader, Investigation of Pt/Al_2O_3 and Pd/Al_2O_3 catalysts for the combustion of methane at low concentrations, Appl. Catal. B 5 (1) (1994) 149–164, http://dx.doi.org/10.1016/0926-3373(94)00037-9.

[68] S.K. Matam, G.L. Chiarello, Y. Lu, A. Weidenkaff, D. Ferri, PdO_x/Pd at work in a model three-way catalyst for methane abatement monitored by operando XANES, Top. Catal. 56 (2013) 239–242, http://dx.doi.org/10.1007/s11244-013-9960-1.

[69] D. Wang, J. Gong, J. Luo, J. Li, K. Kamasamudram, N. Currier, A. Yezerets, Distinct reaction pathways of methane oxidation on different oxidation states over Pd-based three-way catalyst (TWC), Appl. Catal. A: Gen. 572 (2019) 44–50, http://dx.doi.org/10.1016/j.apcata.2018.12.022.

[70] Q. Zhang, L. Lv, J. Zhu, X. Wang, J. Wang, M. Shen, The effect of CO on NO reduction over Pt/Pd-based NSR catalysts at low temperature, Catal. Sci. Technol. 3 (4) (2013) http://dx.doi.org/10.1039/c2cy20775c.

[71] N.W. Cant, D.E. Angove, D.C. Chambers, Nitrous oxide formation during the reaction of simulated exhaust streams over rhodium, platinum and palladium catalysts, Appl. Catal. B 17 (1) (1998) 63–73, http://dx.doi.org/10.1016/S0926-3373(97)00105-7.

[72] H. Wang, Y. Peng, W. Si, C. Gao, Y. Wang, R. Wang, J. Yuan, B. Zhou, J. Li, Influence mechanism of Pd, Pt, Rh/γ-Al_2O_3 on NH_3 formation for NO reduction by CO, Appl. Catal. B 352 (2024) 124009, http://dx.doi.org/10.1016/j.apcatb.2024.124009.

[73] R. Dümpelmann, N.W. Cant, D.L. Trimm, Formation of isocyanic acid during the reaction of mixtures of NO, CO and H_2 over supported platinum catalysts, Appl. Catal. B 6 (4) (1995) 291–296, http://dx.doi.org/10.1016/0926-3373(95)00024-0.

[74] R. Dümpelmann, N.W. Cant, D.L. Trimm, The formation of isocyanic acid (HNCO) by reaction of NO, CO, and H_2 over Pt/SiO_2 and its hydrolysis on alumina, J. Catal. 162 (1) (1996) 96–103, http://dx.doi.org/10.1006/jcat.1996.0263.

[75] N. Macleod, R.M. Lambert, Lean NOx reduction with CO + H_2 mixtures over Pt/Al_2O_3 and Pd/Al_2O_3 catalysts, Appl. Catal. B 35 (4) (2002) 269–279, http://dx.doi.org/10.1016/S0926-3373(01)00264-8.

[76] N. Macleod, R.M. Lambert, An in situ DRIFTS study of efficient lean NOx reduction with H_2 + CO over Pd/Al_2O_3: the key role of transient NCO formation in the subsequent generation of ammonia, Appl. Catal. B 46 (3) (2003) 483–495, http://dx.doi.org/10.1016/s0926-3373(03)00289-3.

[77] D.Q. Phan, S. Kureti, CO oxidation on Pd/Al_2O_3 catalysts under stoichiometric conditions, Top. Catal. 60 (3) (2017) 260–265, http://dx.doi.org/10.1007/s11244-016-0608-9.

[78] V.H. Sandoval, C.E. Gigola, Characterization of Pd and Pd-Pb/α-Al_2O_3 catalysts. A TPR-TPD study, Appl. Catal. A: Gen. 148 (1) (1996) 81–96, http://dx.doi.org/10.1016/S0926-860X(96)00224-4.

[79] H. Dropsch, M. Baerns, CO adsorption on supported Pd catalysts studied by adsorption microcalorimetry and temperature programmed desorption, Appl. Catal. A: Gen. 158 (1–2) (1997) 163–183, http://dx.doi.org/10.1016/S0926-860X(96)00418-8.

[80] K. Foger, J. Anderson, Temperature programmed desorption of carbon monoxide adsorbed on supported platinum catalysts, Appl. Surf. Sci. 2 (3) (1979) 335–351, http://dx.doi.org/10.1016/0378-5963(79)90067-9.

[81] A.S. Lisitsyn, A.S. Kadtsyna, Strong response of Pt clusters to the environment and conditions, formation of metastable states, and simple methods to trace the reversible changes, Phys. Chem. Chem. Phys. 23 (39) (2021) 22718–22732, http://dx.doi.org/10.1039/D1CP01484F.

[82] R.K. Herz, J.B. Kiela, S.P. Marin, Adsorption effects during temperature-programmed desorption of carbon monoxide from supported platinum, J. Catal. 73 (1) (1982) 66–75, http://dx.doi.org/10.1016/0021-9517(82)90081-1.

[83] J.L. Falconer, J.A. Schwarz, Temperature-programmed desorption and reaction: applications to supported catalysts, Catal. Rev. - Sci. Eng. 25 (2) (1983) 141–227, http://dx.doi.org/10.1080/01614948308079666.

[84] J.-W. He, U. Memmert, P.R. Norton, Interaction of oxygen with a Pd (110) surface. II. Kinetics and energetics, J. Chem. Phys. 90 (9) (1989) 5088–5093, http://dx.doi.org/10.1063/1.456551.

[85] M. Milun, P. Pervan, M. Vajić, K. Wandelt, Thermal desorption spectroscopy of the O_2/Pd (110) system, Surf. Sci. 211 (1989) 887–895, http://dx.doi.org/10.1016/0039-6028(89)90854-6.

[86] D.H. Parker, M.E. Bartram, B.E. Koel, Study of high coverages of atomic oxygen on the Pt (111) surface, Surf. Sci. 217 (3) (1989) 489–510, http://dx.doi.org/10.1016/0039-6028(89)90443-3.

[87] R. Chen, Z. Chen, B. Ma, X. Hao, N. Kapur, J. Hyun, K. Cho, B. Shan, CO adsorption on Pt (111) and Pd (111) surfaces: A first-principles based lattice gas Monte-Carlo study, Comput. Theor. Chem. 987 (2012) 77–83, http://dx.doi.org/10.1016/j.comptc.2011.07.015.

[88] D. Childers, A. Saha, N. Schweitzer, R.M. Rioux, J.T. Miller, R.J. Meyer, Correlating heat of adsorption of CO to reaction selectivity: Geometric effects vs electronic effects in neopentane isomerization over Pt and Pd catalysts, ACS Catal. 3 (11) (2013) 2487–2496, http://dx.doi.org/10.1021/cs400527p.

[89] V.A. Drozdov, P.G. Tsyrulnikov, V.V. Popovskii, N.N. Bulgakov, E.M. Moroz, T.G. Galeev, Comparative study of the activity of Al−Pd and Al−Pt catalysts in deep oxidation of hydrocarbons, React. Kinet. Catal. Lett. 27 (2) (1985) 425–427, http://dx.doi.org/10.1007/BF02070487.

[90] M. Shen, M. Yang, J. Wang, J. Wen, M. Zhao, W. Wang, Pd/Support Interface-Promoted Pd−$Ce_{0.7}Zr_{0.3}O_2$−Al_2O_3 Automobile Three-Way Catalysts: Studying the Dynamic Oxygen Storage Capacity and CO, C_3H_8, and NO Conversion, J. Phys. Chem. C 113 (8) (2009) 3212–3221, http://dx.doi.org/10.1021/jp805128u.

[91] H.N. Sharma, V. Sharma, T. Hamzehlouyan, W. Epling, A.B. Mhadeshwar, R. Ramprasad, SOx oxidation kinetics on Pt(111) and Pd(111): First-principles computations meet microkinetic modeling, J. Phys. Chem. C 118 (13) (2014) 6934–6940, http://dx.doi.org/10.1021/jp501538v.

[92] M.V. Twigg, Rôles of catalytic oxidation in control of vehicle exhaust emissions, Catal. Today 117 (4) (2006) 407–418, http://dx.doi.org/10.1016/j.cattod.2006.06.044.

[93] G. Keitl, J. Rink, F. Wen, L. Jongen, A. Hofmann, M. Votsmeier, A. Terfort, J. Gieshoff, Impact of test conditions on the oxygen storage capacity of Pd loaded cerium zirconium oxide, Top. Catal. 60 (3–5) (2017) 272–277, http://dx.doi.org/10.1007/s11244-016-0611-1.

[94] C. Descorme, R. Taha, N. Mouaddib-Moral, D. Duprez, Oxygen storage capacity measurements of three-way catalysts under transient conditions, Appl. Catal. A: Gen. 223 (1–2) (2002) 287–299, http://dx.doi.org/10.1016/S0926-860X(01)00765-7.

[95] G. Ketteler, D.F. Ogletree, H. Bluhm, H. Liu, E.L. Hebenstreit, M. Salmeron, In situ spectroscopic study of the oxidation and reduction of pd (111), J. Am. Chem. Soc. 127 (51) (2005) 18269–18273, http://dx.doi.org/10.1021/ja055754y.

[96] A. Jaree, R.R. Hudgins, H.M. Budman, P.L. Silveston, V.Z. Yakhnin, M. Menzinger, Hysteresis and extinction waves in catalytic CO oxidation caused by reactant concentration perturbations in a packed-bed reactor, Ind. Eng. Chem. Res. 42 (8) (2003) 1662–1673, http://dx.doi.org/10.1021/ie020500w.

[97] C. Huang, W. Shan, Z. Lian, Y. Zhang, H. He, Recent advances in three-way catalysts of natural gas vehicles, Catal. Sci. Technol. 10 (19) (2020) 6407–6419, http://dx.doi.org/10.1039/D0CY01320J.

[98] M. Kaneeda, H. Iizuka, T. Hiratsuka, N. Shinotsuka, M. Arai, Improvement of thermal stability of NO oxidation Pt/Al_2O_3 catalyst by addition of Pd, Appl. Catal. B 90 (3) (2009) 564–569, http://dx.doi.org/10.1016/j.apcatb.2009.04.011.

[99] T. Engel, G. Ertl, Elementary steps in the catalytic oxidation of carbon monoxide on platinum metals, Adv. Catal. 28 (1979) 1–78, http://dx.doi.org/10.1016/S0360-0564(08)60133-9.

[100] K.I. Choi, M.A. Vannice, CO oxidation over Pd and Cu catalysts III. Reduced Al_2O_3-supported Pd, J. Catal. 131 (1) (1991) 1–21, http://dx.doi.org/10.1016/0021-9517(91)90319-Y.

[101] M. Borchers, K. Keller, P. Lott, O. Deutschmann, Selective catalytic reduction of NOx with H_2 for cleaning exhausts of hydrogen engines: Impact of H_2O, O_2, and NO/H_2 ratio, Ind. Eng. Chem. Res. 60 (18) (2021) 6613–6626, http://dx.doi.org/10.1021/acs.iecr.0c05630.

[102] P. Granger, F. Dhainaut, S. Pietrzik, P. Malfoy, A.S. Mamede, L. Leclercq, G. Leclercq, An overview: Comparative kinetic behaviour of Pt, Rh and Pd in the NO + CO and NO + H_2 reactions, Top. Catal. 39 (1–2) (2006) 65–76, http://dx.doi.org/10.1007/s11244-006-0039-0.

[103] E.C. Adams, M. Skoglundh, T. Elmøe, P.-A. Carlsson, Water–gas-shift assisted ammonia formation over Pd/Ce/alumina, Catal. Today 307 (2018) 169–174, http://dx.doi.org/10.1016/j.cattod.2017.05.035.

[104] T. Engel, A molecular beam investigation of He, CO, and O_2 scattering from Pd(111), J. Chem. Phys. 69 (1) (1978) 373–385, http://dx.doi.org/10.1063/1.436363.

[105] G.R. Pesch, N. Riefler, U. Fritsching, L. Colombi Ciacchi, L. Mädler, Gas-solid catalytic reactions with an extended DSMC model, AlChE J. 61 (7) (2015) 2092–2103, http://dx.doi.org/10.1002/aic.14856.

[106] J. Ratcliff, K. Karinshak, M.P. Harold, Rich methane oxidation on Pt/Pd/Al_2O_3: Steady state performance, multiplicity features, and spatial patterns, Chem. Eng. Sci. 282 (2023) http://dx.doi.org/10.1016/j.ces.2023.119269.